5th AIAA Propulsion Aerodynamic Workshop 2020
PAW05 – Rectangular Exhaust Nozzle

Revised March 20, 2020

Guidelines/Instructions for Participation in PAW05

1. Objectives: The main objective the 5th Propulsion Aerodynamics Workshop (PAW05) nozzle test case is to assess the accuracy of existing computer codes and modeling techniques in simulating the aerodynamics and thermodynamics of complex nozzle exhaust flows. Previous workshops focused on nozzle aerodynamics and propulsion efficiency metrics. The PAW05 nozzle configuration under investigation will focus on a heated jet exhaust and interaction with a film cooled surface downstream of the nozzle exit.

   The degree of success of these simulations will be judged against measurements of velocities and temperatures in the jet issuing from a convergent nozzle over a film cooled surface. The velocities were measured using particle image velocimetry (PIV) and temperatures were measured using spontaneous rotational Raman scattering (SRS) spectroscopy. Additionally, thermocouple data and IR images will be used for comparison.

   The expected standard computational analysis technique is Reynolds-averaged Navier-Stokes (RANS). Due to the complexity of the flow and heat transfer problem under consideration, participants are also encouraged to expand beyond RANS with different turbulence modeling approaches including URANS, DES, and LES. Various thermal modeling approaches, possibly conjugate heat transfer or equivalent techniques, are of key interest to the committee and creativity is encouraged in developing heat transfer approaches for the deck. However, adiabatic or specified wall temperature solutions will also be accepted.

   Four levels of unstructured grid refinement will be provided to workshop participants as well as the test geometry. Note, the provided grids discretize the fluid domain only. Participants will be responsible for discretizing and reporting grid information on the solid domain if conjugate heat transfer methods are applied. If participants create their own grids for the fluid simulation, please report the grid information used.

2. Nozzle configuration: The test article under consideration is a convergent nozzle attached to a plenum with a cooled plate, as shown in Figure 1. The entire assembly was fabricated from 316 stainless steel. The nozzle transitions from a 152.4 mm radius round cross-section through a series of super ellipses to a square nozzle with 68.07 mm sides at the nozzle exit. This square nozzle exit shape was chosen in order to provide a volume of uniform flow over the plate surface where the hot exhaust interacted with the injection stream. The dimension of 68.07 by 68.07 mm exit area was determined to

be the largest that would correspond to a nozzle mass flow that would not overly strain the flow and fuel supply systems of NASA Glenn's Small Hot Jet Acoustic Rig (SHJAR). See Figures 1 and 2 for schematic drawings of the test hardware. The nozzle internal contour was designed to have a continually decreasing cross sectional area while moving downstream, except for the last 25.4 mm before the nozzle exit, to enable a favorable pressure gradient, and in turn, minimal secondary flows at the nozzle exit.

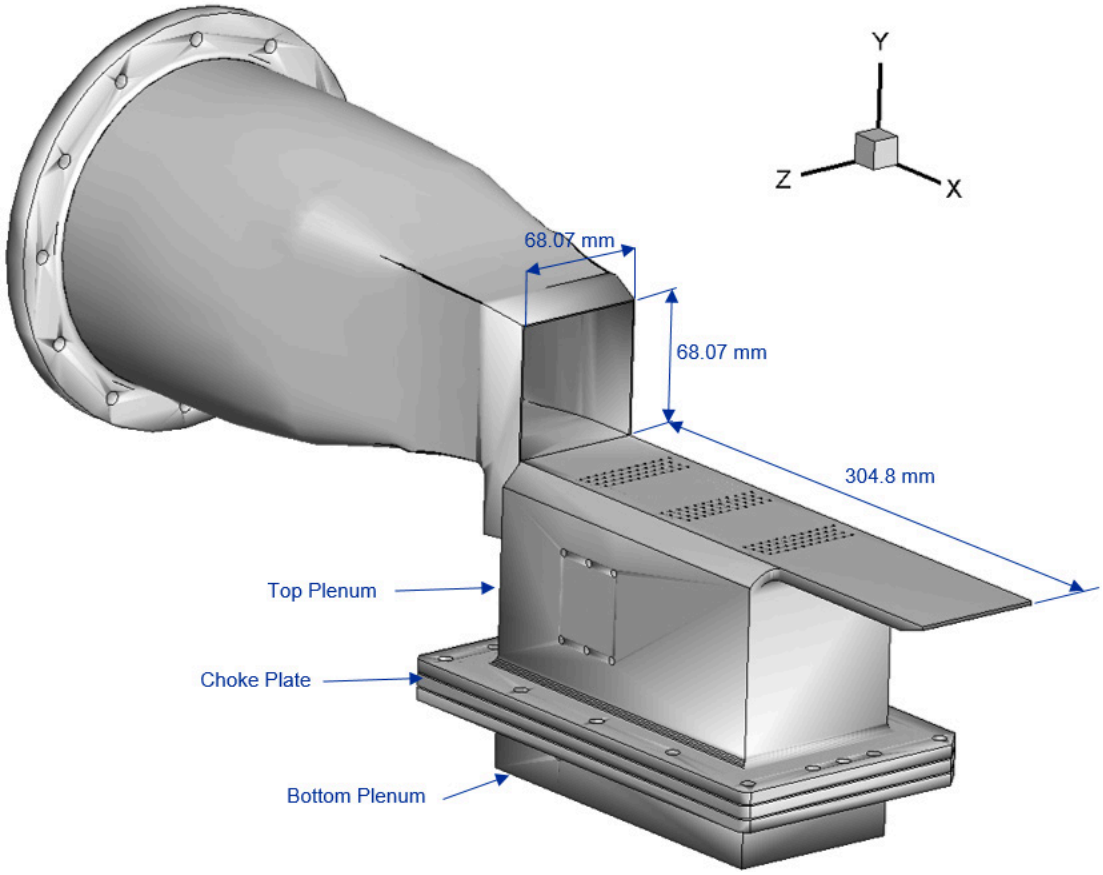

Figure 1.—Experimental configuration – square nozzle with the 6.35 mm thick plate and three patches of forty–five 1 mm (drilled to 0.040 inch) diameter injector holes angled at 30° to plate surface. Cooling air is provided by the two chamber plenum.

A flat plate or deck was mounted to the square nozzle to form the nozzle/deck assembly, see Figure 1. The 6.35 mm thick plate spans the width of the nozzle exit (68.07 mm) and extends 304.8 mm axially from the nozzle exit, ending with a 15° taper. The plate was equipped with three separate patches of 45 holes (135 holes in total) arranged in a staggered pattern, as shown in Figure 2 with intra-hole spacings of $\Delta X/D$ = 5 and $\Delta Z/D$ = 5. The Z-offset of each successive row is Z/D = 1.25. The cooling holes were 1 mm in diameter (actually machine drilled to a specification of 0.040 inches with 0.001 tolerance) and inclined 30° from the horizontal, yielding an L/D = 12.5. The cooling air flow was delivered to the plate via a dual chambered plenum assembly, in order to provide a uniform cooling air supply from the bottom side of the perforated plate at a

constant blowing ratio for the three patches of holes. The unheated shop air cooling flow entered the high pressure bottom plenum through a 12.7 mm orifice. A choke plate with thirty-two 0.78 mm diameter holes arranged in a 4×8 regular grid pattern (X/D = Z/D = 25.8) was used to provide a uniform flow and pressure field below the cooling holes in the top plate. The height of the low pressure plenum was designed to provide adequate distance for the individual jets from the choke plate to mix into a uniform volume of nearly quiescent air below the deck. The highest pressure differential observed across the choke plate was 10:1 for the highest blowing ratios used in this study. The top and bottom plenums were designed with 6.35 mm thick walls to ensure structural integrity of the model under the full range of blowing ratios. In order to accommodate the 6.35 mm plenum walls, the top chamber was wider than the top plate surface. This resulted in the 45° bevel along the sides of the plate. A total of 17 thermocouples (T_cs) were embedded along the length of the plate extending from the nozzle exit, shown as the red dots in Figure 2. Note that just behind each of the first and second patches of cooling holes, there is a single T_c measuring temperature at the top of the plate (solid red circle). Adjacent to this is a second T_c at the same axial station but staggered 12.7 mm (0.50 inches) in the spanwise direction, measuring temperature on the underside of the plate. The purpose of these two T_c pairs was to be able to get an estimate of temperature gradient from the top to bottom of the plate across the 6.35 mm plate thickness.

3. Flow Conditions and Nozzle Operation: Table 1 gives the operating points that will be used as workshop test cases. Reference 1 contains results for two other set points (23 and 49) which can be used by participants to anchor their solutions. Data for set point 42 has not yet been published. The highest blowing ratios were achieved for set point 42, because the maximum cooling air that could be delivered to the system was limited, and the nozzle flow for set point 42 was the lowest.

Table 1. Operating Conditions

Set Point	TR	NPR	M_j	BR	Nozzle mass flow rate (kg/s)	Injector mass flow rate (kg/s)
42	2.7	1.066	0.304	0.0	0.34	0.0
42	2.7	1.066	0.304	1.0	0.34	0.0081
42	2.7	1.066	0.304	2.0	0.34	0.0162

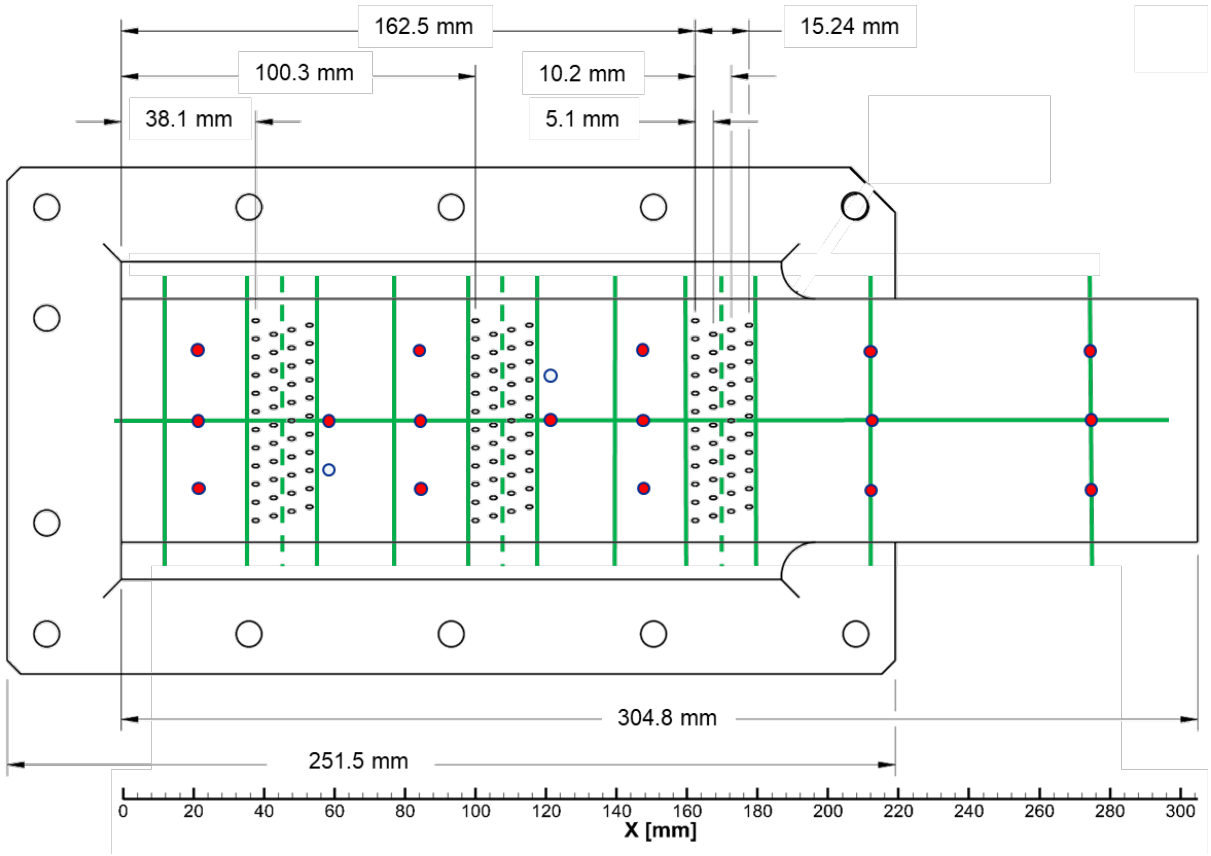

Figure 2.—Top view of the plate showing the cooling hole geometry and dimensions. The red circles indicate the Tc locations embedded in the top surface of the plate. The empty blue circles indicate the locations of the Tcs on the underside of the plate. The green lines show the planes where PIV data were collected. Raman temperature surveys were performed at the intersections of the solid green lines and the centerline streamwise PIV plane. The scale on the bottom provides a reference for the axial locations of the Raman, T_c and PIV measurements.

The nozzle was operated by controlling the supply total pressure to achieve the jet exit Mach number (Mj) corresponding to a given nozzle pressure ratio (NPR = supply total pressure divided by ambient static pressure) and nozzle static temperature ratio (TR = calculated jet exit static temperature divided by ambient static temperature). It is standard in many aerodynamic CFD simulations to assume a calorically perfect gas, such that the specific heat ratio, γ, is constant, and if the working fluid is air, $\gamma = 1.4$. The NPR and calculated jet Mach number, M_j, shown in Table 1 assumes $\gamma = 1.4$. For the calculations to be obtained for these workshop cases, this is probably an acceptable assumption, and employing a variable γ capability will not likely change the results significantly. In the test, hydrogen was combusted to heat the air to the desired

temperature. For those interested in simulating gas properties other than air, please contact the committee and those conditions will be supplied. The primary effects are to reduce the nozzle flow rate slightly and to change the gas properties slightly with presence of H_2O in the exhaust gas. The nozzle inflow total temperature may be set using the same assumption. Using the set point 42 case in the table, a static temperature ratio of 2.7, would correspond to a nozzle total temperature ratio (NTR) = 2.75. The nozzle operating conditions that were held fixed were TR and M_j. See the boundary condition section for discussion on typical freestream / reference conditions.

For the cooling plenum, unheated shop air was supplied to the high pressure plenum (shown as "bottom plenum") in Figure 1. The blowing ratio, BR, is based on total mass flow rates and areas of the nozzle and injector exit areas = $(m_{inj}/m_j)\cdot(A_j/A_{inj}) \sim (\rho U)_{inj}/(\rho U)_j$. The nozzle has relatively flat exit profiles of velocity, temperature, and density, and profiles were measured in the experimental program at 12.7 mm downstream of the nozzle exit. Preliminary RANS simulations of the same nozzle, but with a single cooling hole configuration, conducted in Reference 2, showed that a fully turbulent flow simulation with a standard two-equation model would yield velocity and temperature boundary layer profiles that matched experimental data at this first axial measurement station. The "$(\rho U)_{inj}$" quantity in these multi-hole experiments is the total mass flow exiting the 135 holes divided by the total cooling hole cross sectional area.

4. Boundary Conditions: As discussed in the previous section, assuming $\gamma = 1.4$ for all cases will probably yield results that will not deviate far from the calorically imperfect assumption. This is especially the case if comparisons of solutions and experimental data are made on a nondimensional basis.
    a. For the nozzle, holding inflow total pressure and temperature to values derived from Table 1 is sufficient. For RANS simulations with linear two-equation turbulence models, no special inflow turbulence state should be necessary, and performing the simulation as fully turbulent from the inflow should yield boundary layer growth that matches experimental data at the first measurement station downstream of the nozzle exit.
    b. The best set of boundary conditions for the plenum probably consists of the overall cooling mass flow rate and plenum temperature. For completeness, it is noted that for the BR=1 case, the plenum pressure was approximately 109.7 kPa and for BR=2, the pressure was approximately 126.6 kPa. While the cooling plenum is unheated, the bulk temperature in the plenum below the plate was measured to be about 34 K higher than ambient for the BR=1 case and 17 K higher than ambient for the BR=2 case.
    c. Wall boundary conditions may be set to adiabatic or the participant's choice of heat transfer approach.
    d. Inflow boundaries for the nozzle and plenum may include specification of the turbulence viscosity ratio, which can be set to a nominal value ~5 to simulate the expected low turbulence levels expected to enter the domain.

e. While there was some small variation in flow conditions from day to day, and even within a day, freestream condition of 99.0 kPA and 300 K should represent the test conditions well.

5. Required Submission Data: The organizing committee will provide an ASCII template for submission of the following data. Data sets for the two blowing ratios = 1.0, and 2.0 are required on each grid level. In addition, it is recommended that data for BR = 0.0 also be supplied. Data should be provided to the committee one month before the workshop to guarantee inclusion in the summary analysis.
    a. Plate surface temperature along the axial centerline averaged over a 0.5 inch spanwise width at each axial data location.
    b. Velocity and thermal boundary layer profiles at centerline axial locations where 3 spanwise temperature measurements were made downstream of the first set of cooling holes: x=76.8 mm (3.02 in), 138.4 mm (5.45 in), 208.0 mm (8.20 in), and 270.3 mm (10.64 in).
    c. Mass flow rates at the nozzle and plenum entrance planes.
    d. Viscous forces on the plate in the form of integrated drag.
    e. Total heat flux on the plate.
    f. Top-down view of plate surface temperature for comparison to IR camera images. Tecplot or Fieldview templates will be provided.
    g. Code efficiency in form of [total wall clock time/number of processors/number of grid points].
    h. General solver information (turbulence model, discretization type [cell-centered/node-centered], heat transfer model, film cooling model, etc).

References

1. Wernet, M.P., Georgiadis, N.J., Locke, R.J., Thurman, D.R., and Poinsatte, P.E., "PIV and Rotational Raman-Based Temperature Measurements for CFD Validation of a Perforated Cooling Flow – Part 1, AIAA Paper 2020-1230, Jan. 2020. Also NASA TM 2019-220227, July 2019.
2. Wernet, M.P., Georgiadis, N.J., and Locke, R.J., "PIV and Rotational Raman-Based Temperature Measurements for CFD Validation in a Single Injector Cooling Flow," AIAA Paper 2018-3857 and NASA TM 2018-219739, Jan. 2018.